Device variability and circuit redundancy in signal processing based on nanoswitches

2009 Nanotechnology 20 465202

(http://iopscience.iop.org/0957-4484/20/46/465202)

Nanotechnology **20** (2009) 465202 (8pp) doi:10.1088/0957-4484/20/46/465202

Device variability and circuit redundancy in signal processing based on nanoswitches

Javier Cervera, José A Manzanares and Salvador Mafé

Facultat de Física, Universitat de València, E-46100 Burjassot, Spain

E-mail: Javier.Cervera@uv.es

Received 20 July 2009, in final form 9 September 2009
Published 22 October 2009
Online at stacks.iop.org/Nano/20/465202

Abstract

Signal processing based on molecular switches whose conductance can be tuned by an external stimulus between two (*on* and *off*) states has been proposed recently (Cervera *et al* 2008 *J. Appl. Phys.* **104** 084317). The basic building block is a metal nanoparticle linked to two electrodes by an organic ligand and a nanoswitch. The net charge delivered by this nanostructure exhibits a sharp resonance when the alternating potential applied between the electrodes has the same frequency as the periodic variation between the *on* and *off* conductance states induced on the nanoswitch. This resonance can be used to process an external signal by selectively extracting the weight of the different harmonics. However, because of the fabrication process at the nanoscale, the nanostructures will show a significant variability in the physical characteristics. By using a phenomenological model that includes this variability, the stochastic nature of electron transference, and the thermal noise, we demonstrate that reliable signal processing can still be achieved by adapting the number of nanoswitches per bit of information (circuit redundancy) to the nanostructure tolerance (device variability). Extensive kinetic Monte Carlo simulations show that a moderate level of redundancy can compensate for significant nanostructure variability. This result gives support to the concept of ensembles of redundant switches as reliable components for signal processing at the nanoscale.

(Some figures in this article are in colour only in the electronic version)

1. Introduction

Switches are central to information processing. In particular, nanostructures showing externally-tuneable high (*on*) and low (*off*) conductance states are of interest as the building blocks of molecular electronics [1–5]. The switching can be accomplished by conformational or redox changes [1–3] induced by exposition to light [6–10], an electrochemical reaction [2, 11, 12] or a mixed photochemical/electrochemical process [13, 14]. Multi-atom relay [15] and nanoscale Si-based [16] resistance switching devices, Langmuir–Blodgett monolayers with large *on*/*off* resistance ratios [17–19], and nanoscale field-effect transistors [20] have also been demonstrated experimentally. Other nanostructures of recent interest are quantized-conductance atomic switches based on mixed electronic and ionic conductors [4], nanoscale solid-electrolyte devices [5], and memristive systems formed by nanoparticle assemblies that show an abrupt and large resistance switching at room temperature [21]. Because the list of chemically, physically and electrochemically switchable nanostructures is expanding rapidly [22], theoretical studies proposing novel information processing schemes based on these systems can stimulate future particular realizations by showing the essential characteristics of the concept.

Monolayer-protected metal nanoparticles [23–28] can be employed to optimize the electron transfer between the electrodes and the switching molecule [29, 30]. We have explored recently the use of molecular switches to implement a signal processing scheme based on the sharp resonance of the net charge delivered by a nanoparticle linked to two electrodes by a nanoswitch and an organic ligand [30]. The nanoswitch has an active centre permitting to tune the conductance between the values G_M (maximum) and G_m (minimum) using a switching electrode or a light pulse. The resonance occurs when the frequency of the alternating potential applied between the electrodes is equal to that of the periodic conductance variation induced on the nanoswitch. This property allows for decoding a global input signal by extracting the weight of the different harmonics.

Metal nanoparticles with organic ligands are usually a few nanometres in diameter. Tunnelling is the dominant conduction mechanism through the alkanethiol ligands [31, 32], although the nature of the electrical contacts in the molecular junctions is also important [32]. Electron transfer is influenced by the discrete nature of charge transport and the Coulomb blockade energy barrier associated with the nanoparticle when the Coulombic energy is higher than the thermal energy. This condition is usually fulfilled by scaling down the elementary building blocks. However, nanostructures [33, 34] suffer from tolerance problems (because of the variability in their physical characteristics) that may affect reliable operation. In particular, the size distribution of the metal nanoparticles [35] results in a significant spread of their properties. It has been reported that high parameter variability influences the conductance of molecular memories [36], the threshold potential of voltage-driven molecular switches [37], and the tunnelling junction characteristics of disordered arrays [38]. Fault-tolerant approaches [36, 39, 40] are needed to perform reliable information processing from inherently unreliable nanodevices.

Previous proposals for information processing using nanostructures have emphasized memory and logic gate schemes [41–54] and paid limited attention to the issue of variability. In this study, we consider frequency-dependent signal processing [30, 55] using nanoswitches with significant variability and analyse the general properties required for practical implementation. We carry out kinetic Monte Carlo simulations [55] for a broad range of conditions and compare the results obtained with those resulting from deterministic approaches based on the master equation [30] to better understand the stochastic nature of electron transfer and the thermal noise effects. Moreover, we show that the introduction of a moderate circuit redundancy can compensate for the nanostructure variability, which is an important step towards practical implementation of signal processing schemes based on these systems.

2. Theoretical modelling

The building block of the signal processing device is formed by a metal nanoparticle linked to two electrodes by a nanoswitch and an organic ligand [30] (see figure 1(a)). Figure 1(b) shows the equivalent circuit of the nanostructure, which includes the left (L) and right (R) resistances $R_L = 1/G_L$ and $R_R = 1/G_R$, the capacitances C_L and C_R, and the electron transfer rates $\Gamma^{\pm}_{L,n}$ and $\Gamma^{\pm}_{R,n}$. The time-dependent drain to source (or bias) voltage is $V(t)$. A gate voltage V_G can also be applied to the nanoparticle connected to the gate capacitance C_G. (While the use of this gate electrode is usual, it is not essential for the device performance at high temperature [30].) Electron transfer occurs by tunnelling between the electrodes and the nanoparticle, and it is modulated by the ligands. The nanoswitch has an active centre allowing to tune externally the left conductance G_L between the values G_M (maximum) and G_m (minimum) using a switching electrode or a light pulse.

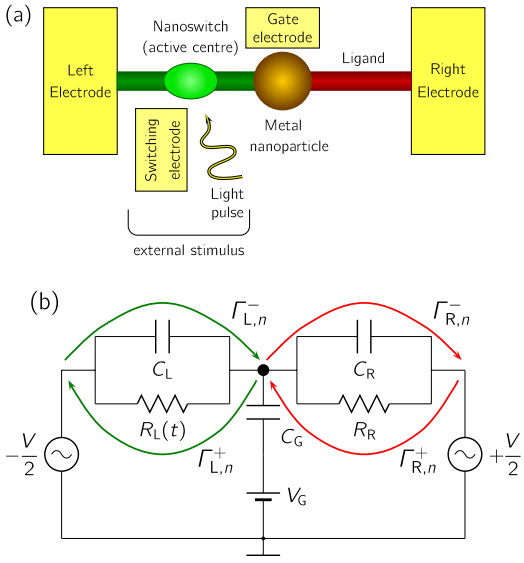

Figure 1. (a) The building block of the signal processing scheme is a nanostructure formed by a metal nanoparticle linked to two electrodes by a molecular switch and an organic ligand (in red). The nanoswitch has an active centre that permits to modulate its conductance between the values G_M and G_m by means of an external stimulus (e.g., a switching electrode or a light pulse) [30].
(b) Equivalent circuit of this nanostructure, showing left (L) and right (R) resistances, capacitances, and electron transfer rates. A voltage V_G can be also applied to the gate electrode and its influence on the nanoparticle is given by the gate capacitance C_G.

We assume that the left conductance can be modulated periodically with a frequency $\nu_0 = 1/\tau$:

$$G_L(t) = \begin{cases} G_m, & 0 < t < \tau/2 \\ G_M, & \tau/2 < t < \tau. \end{cases} \tag{1}$$

When $h\nu_0 < kT$, the electron tunnelling rates are [30, 56]:

$$\Gamma^{\pm}_{L,n}(t) = \frac{G_L(t)}{e^2} \frac{-\Delta E^{\pm}_{L,n}}{1 - \exp(\Delta E^{\pm}_{L,n}/kT)} \tag{2}$$

$$\Gamma^{\pm}_{R,n}(t) = \frac{G_R}{e^2} \frac{-\Delta E^{\pm}_{R,n}}{1 - \exp(\Delta E^{\pm}_{R,n}/kT)} \tag{3}$$

where $\Gamma^{\pm}_{L,n}$ and $\Gamma^{\pm}_{R,n}$ are the tunnelling rates for electron transitions between the left (L) and right (R) electrodes and the nanoparticle from left to right (−) and from right to left (+), as shown in figure 1(b). $\Delta E^{\pm}_{L,n}$ and $\Delta E^{\pm}_{R,n}$ are the changes in electrostatic energy between the electronic occupation states n and $n+1$ of the nanoparticle. The electrons are localized inside the nanoparticle because the conductances G_L and G_R are much smaller than the quantum conductance $G_0 = 2e^2/h = 77.4\ \mu$S, where e is the elementary charge and h is the Planck constant. This permits the estimation of $\Delta E^{\pm}_{L,n}$ and $\Delta E^{\pm}_{R,n}$ using the orthodox theory [56–58]:

$$\Delta E^{\pm}_{L,n}(t) = \mp \frac{e^2}{C_\Sigma} \left[\frac{1}{2} + n - \frac{C_G V_G}{e} - \frac{(C_R + C_G/2)V}{e} \right] \tag{4}$$

$$\Delta E^{\pm}_{\mathrm{R},n}(t) = \pm\frac{e^2}{C_\Sigma}\left[\frac{1}{2} + n - \frac{C_\mathrm{G}V_\mathrm{G}}{e} + \frac{(C_\mathrm{L}+C_\mathrm{G}/2)V}{e}\right] \tag{5}$$

where $Q_\mathrm{G} = C_\mathrm{G}V_\mathrm{G}$ is the charge injected to the nanoparticle by the gate electrode and $C_\Sigma = C_\mathrm{L} + C_\mathrm{R} + C_\mathrm{G}$ is the total capacitance.

Using the master equation formalism the occupation state of the nanoparticle is evaluated from [30, 58]:

$$\frac{\mathrm{d}P_n}{\mathrm{d}t} = (\Gamma^-_{\mathrm{L},n-1} + \Gamma^+_{\mathrm{R},n-1})P_{n-1} + (\Gamma^+_{\mathrm{L},n} + \Gamma^-_{\mathrm{R},n})P_{n+1} - (\Gamma^+_{\mathrm{L},n-1} + \Gamma^-_{\mathrm{R},n-1} + \Gamma^-_{\mathrm{L},n} + \Gamma^+_{\mathrm{R},n})P_n \tag{6}$$

where $P_n(t)$ is the probability of the occupation state n. Initially, $P_0(0) = 1$ and $P_n(0) = 0$ $(n > 0)$ because no electrons have been transferred to the nanoparticle. From the time evolution of the probabilities $P_n(t)$, the current

$$I(t) = -e\sum_n [\Gamma^-_{\mathrm{L},n}P_n(t) - \Gamma^+_{\mathrm{L},n}P_{n+1}(t)] \tag{7}$$

and the net charge delivered after a retrieval time t_0

$$Q = \int_0^{t_0} I(t)\,\mathrm{d}t \tag{8}$$

are calculated. We use Q to assess the feasibility and performance of the signal processing scheme because Q could be detected by using output capacitors of relatively large capacitances as interfaces between the nanostructure and a CMOS circuit (these capacitors would give observable time-dependent potentials [50, 59]). However, current noise can severely limit the practical operation [30, 58, 59] and we estimate current fluctuations by using the Full Counting Statistics approach, which gives an evaluation of the probability distribution function of the electrons transferred to a given electrode [60, 61]. The second moment of this distribution corresponds to the fluctuations in the net charge delivered, $\langle(Q - \langle Q\rangle)^2\rangle$, from which we estimate $\Delta^* Q = \sqrt{\langle(Q - \langle Q\rangle)^2\rangle}$ as the uncertainty of $\langle Q\rangle$.

To check the validity of the above (continuum and deterministic) model of electron transfer based on the master equation, we have used also a kinetic Monte Carlo algorithm where the electronic rates are given by the semi-classical orthodox theory [55], incorporating explicitly the stochastic nature of the electron transfer through the nanostructure.

Figure 2(a) shows the net charge delivered by the nanostructure as a function of the dimensionless frequency of the applied potential $V(t) = V_0\sin(2\pi\nu t)$. The capacitances of the ligands are $C_\mathrm{L} = C_\mathrm{R} = 1$ aF. The conductances are $G_\mathrm{R} = 100$ nS for the right ligand, and $G_\mathrm{M} = 10$ nS and $G_\mathrm{m} = 5$ nS for the *on* and *off* states of the nanoswitch. The capacitance and potential of the gate electrode are $C_\mathrm{G} = 4$ aF and $V_\mathrm{G} = 20$ mV. These values are typical of nanostructures [2, 25–27, 30, 41, 51, 57–59]. The additional parameters $V_0 = 1$ mV, $t_0 = 1$ ms, and $T = 300$ K are used throughout this study. The conductance switching frequency in equation (1) is $\nu_0 = 10^5$ s^{-1}. To obtain an efficient modulation of conductance G_L, this frequency must be lower than the characteristic relaxation frequency for the change in the nanoswitch conductance. We need to consider also the characteristic sampling frequency bandwidth of the detector, which may limit the frequencies used for conductance modulation in practical operation. In any case, the system can operate also at much lower frequencies (because the switching frequency is set externally). The drawback of a lower frequency is the longer operational time t_0, albeit with a higher signal-to-noise ratio [30].

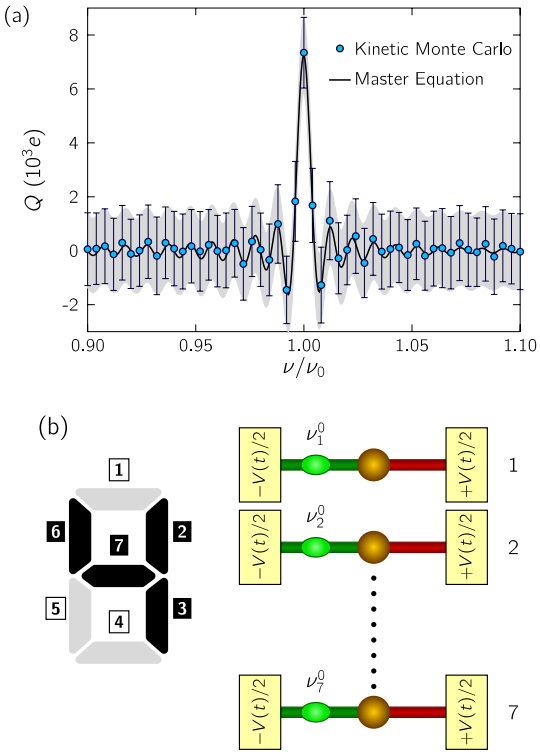

Figure 2. (a) Net charge delivered after $t_0 = 1$ ms by the nanostructure of figure 1(a) as a function of the ratio between the frequency ν of the potential $V(t) = V_0\sin(2\pi\nu t)$ applied between the electrodes and the frequency ν_0 of the conductance modulation. A resonance occurs when $\nu = \nu_0$. The continuous curve, calculated using the master equation, constitutes a good approximation to the points obtained using a kinetic Monte Carlo algorithm. The error bars of these points are noise estimations calculated from the mean square deviation of the charge Q. The shadow region describes the uncertainty in Q obtained from the master equation. (b) Each nanostructure of figure 1 represents a bit of the seven-bit pattern shown in the figure. The pattern 4 is defined by the vector $\mathbf{a} = (0, 1, 1, 0, 0, 1, 1)$ and introduced through the applied potential $V(t) = V_0\sum_{i=1}^{7} a_i\sin(2\pi\nu_i^0 t)$. The net charge Q_i delivered by nanostructure i determines the bit state (*black* or *white*).

Figure 2(a) shows a marked resonance in the charge delivered when the frequencies of the conductance modulation (ν_0) and the applied potential (ν) are equal. The resonance peak is more marked for large nanoswitch conductance ratios $G_\mathrm{m}/G_\mathrm{M}$ and increases with the time t_0 and the potential amplitude V_0 [30]. The continuous curve calculated using the master equation approach constitutes a good approximation to the points obtained with the kinetic Monte Carlo algorithm. The bars on each point are estimations of the thermal noise calculated from the mean square deviation of Q. A signal processing device can be implemented on the basis of the

resonance shown in figure 2(a) [30]. We consider a seven-segment pattern, where the segments (or bits) can be in *black* or *white* states. The proposed signal processing device is formed by the parallel arrangement of seven nanostructures shown schematically in figure 2(b), where every nanostructure represents a bit. Using this arrangement, a pattern codified as input vector $\mathbf{a} = (a_1, a_2, \ldots, a_7)$ that stores the bit states ($a_i = 1$ for black state and $a_i = 0$ for white state) can be recognized. For instance, the input vector corresponding to the pattern 4 shown in figure 2(b) is $\mathbf{a} = (0, 1, 1, 0, 0, 1, 1)$. The switching function of equation (1) is applied to the switch of nanostructure i with frequency ν_i^0, and the neighbouring nanostructures have switching frequencies that differ in a factor 2, $2\nu_{i-1}^0 = \nu_i^0 = \nu_{i+1}^0/2$; and $\nu_1^0 = 10^5\ \mathrm{s}^{-1}$. When the parallel arrangement is fed with the *global* input potential

$$V(t) = V_0 \sum_{i=1}^{7} a_i \sin(2\pi \nu_i^0 t) \tag{9}$$

a resonant response is induced only on those nanostructures where $a_i = 1$ (see figure 2(a)). In this way, the nanostructures with $a_i = 1$ deliver a higher net charge Q_i than those with $a_i = 0$. A threshold charge can be established to identify (beyond the uncertainty introduced by the noise) the nanostructures having a resonant response. The net charge Q_i determines the state of bit i ($i = 1, \ldots, 7$) to be black if Q_i is above the threshold and white otherwise. This allows us to decode the input signal by extracting the state of the different harmonics, retrieving correctly the value of the input vector **a** under a wide range of experimental conditions (temperature, potential, conductance ratio, and retrieval time) [30]. This signal processing device makes use of the concept of resonance discussed by Pistolesi and Fazio [58]. However, it differs significantly from previous studies on oscillating electromechanical nanostructures [58, 62, 63].

The proposed signal processing scheme relies on the fact that the net charge delivered by a nanostructure is a cumulative property, relatively robust with respect to fluctuations. However, thermal noise may impose limitations on the device reliability because it increases the uncertainty of the net charge delivered by each nanostructure. This may cast some doubts on whether Q_i is above or below the threshold value. The experimental variability in the nanostructure characteristics, which is inherent to the nanoscale, increases further the uncertainty of Q_i and might render the device inoperative.

The effect of thermal noise was analysed previously using the master equation approach [30]. We extend significantly this preliminary study by incorporating also the effect of the nanostructure variability on the signal processing. First, truncated Gaussian distributions are introduced to describe the experimental variability of every nanostructure characteristic ($G_\mathrm{m}, G_\mathrm{M}, G_\mathrm{R}, C_\mathrm{R}, C_\mathrm{L}$, and C_G), contrary to our previous work that assumed these values to be free from tolerance problems. Second, the electron transfer is modelled using a kinetic Monte Carlo algorithm, which constitutes a more efficient approach than the master equation formalism when the nanostructures have different characteristics. And third,

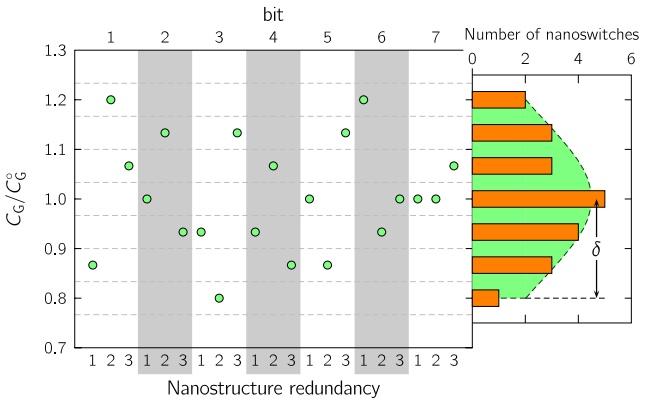

Figure 3. To account for the nanostructure variability, the gate capacitance values $C_{\mathrm{G},ij}$ of $7M = 21$ nanostructures are randomly distributed using a truncated Gaussian distribution around the mean value C_G^0. The distribution is limited by a variability width $\delta = 0.2$ ($1 - \delta \leqslant C_{\mathrm{G},ij}/C_\mathrm{G}^0 \leqslant 1 + \delta$). Index i makes reference to the bit number and index j denotes the redundant nanostructure number in a given bit.

the concept of circuit redundancy is demonstrated as a feasible solution to the thermal noise and device variability problems.

Taking advantage of the scalability properties of nanostructures, we show that a better discrimination between the Q_i values (and hence an improved signal processing) can be achieved by introducing a certain degree of circuit redundancy. The concept of redundancy was considered by von Neumann [64] to build early computers using unreliable components, and it has been suggested recently that the use of redundant architectures may be necessary at the nanoscale [65, 66]. We extend the original signal processing scheme by using a parallel arrangement of $M \geqslant 1$ redundant nanostructures per bit instead of only one (figure 2(b)), where M is the circuit redundancy. We assume that the conductances $G_{\mathrm{L},ij}$ of the $j = 1, \ldots, M$ redundant nanostructures that compose bit i are modulated with the same frequency ν_i^0. The pattern is still defined by the vector **a** and introduced through the applied potential $V(t)$ of equation (9). The net charge $Q_i = \sum_{j=1}^{M} Q_{ij}$ delivered by the M redundant nanostructures composing bit i ($i = 1, \ldots, 7$) now determines the bit state (black or white).

Metal nanoparticles [35, 67–70] and nanowires [71] show Gaussian-like distributions in the size dimensions. This variability affects the electrical properties of the nanostructures that compose the signal processing system. Different nanoparticle radii, for example, will lead to a finite distribution of the resulting capacitances because the two magnitudes are related (an approximately spherical capacitor has a capacitance that scales linearly with its radius). Similarly, when the size dimension and position of the ligands connecting the nanoparticle to the electrodes suffer from a significant variability, this will be reflected in the variability of the tunnelling resistances [72–74]. Also, the effect of a secondary gate depends on the distance and position with respect to the nanoparticle and then the gate capacitances will follow a distribution similar to those of the other parameters. To describe the effect of the variability on the system parameters we employ a truncated Gaussian distribution (see figure 3),

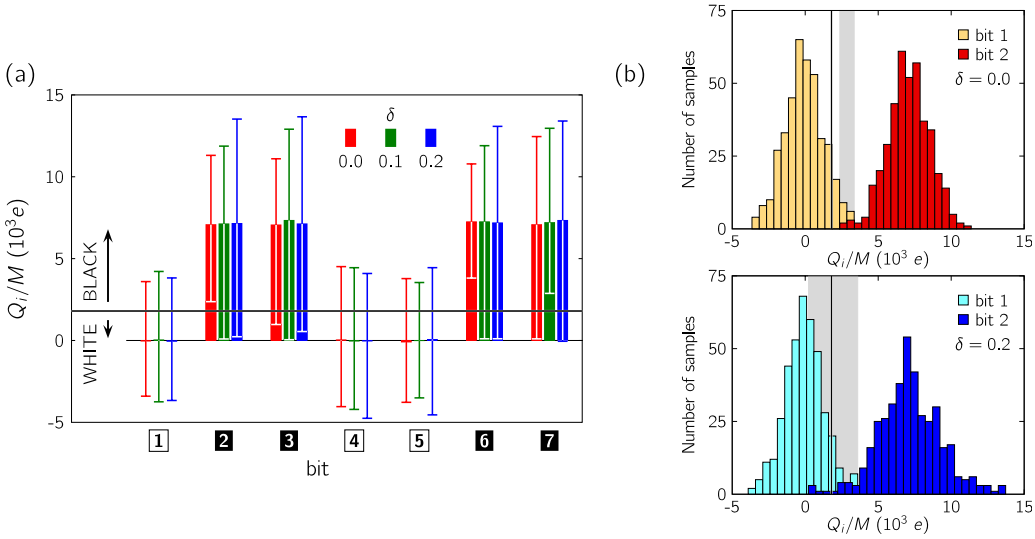

Figure 4. (a) Net charge delivered per nanostructure for variability $\delta = 0$, 0.1, and 0.2 with no redundancy ($M = 1$). The vertical bars are the mean values of the Q_i distributions and the error bars indicate the width of the distributions. The bit state is retrieved as *black* when the value of Q_i is above the threshold (indicated by the black horizontal line) and retrieved as *white* otherwise. (b) Distributions of charges Q_1 and Q_2 delivered by nanostructures 1 (*white*) and 2 (*black*) obtained with 400 simulation runs for $\delta = 0$ and 0.2. Significant overlapping (and thus poor signal processing) occurs for high component variability ($\delta = 0.2$) and no redundancy. The overlapping region of the distribution tails of Q_1 and Q_2 is shown as a grey vertical strip. The black vertical line is the threshold charge.

assuming as a first approximation that this variability affects all the parameters that depend on the size and position of the nanoparticles, the ligands and the gate (the tunnelling resistances described by the conductances G_R, G_M, and G_m, the capacitances C_L and C_R, and the gate capacitance C_G).

In all the simulations carried out, the $7M$ values of every nanostructure characteristic are randomly generated using a truncated Gaussian distribution with prescribed standard deviations around the typical nanoscale mean values $G^0_m = 5$ nS, $G^0_M = 10$ nS, $G^0_R = 100$ nS, $C^0_R = C^0_L = 1$ aF, and $C^0_G = 4$ aF. Every distribution is limited by a variability width, δ, which describes the maximum relative variation of the nanostructure characteristic with respect to the mean value (see figure 3). We note that each Gaussian distribution describes the complete set of $7M$ nanostructures composing the signal processing device, not the M redundant nanostructures of a particular bit. For example, figure 3 shows a distribution of 21 gate capacitance values ($C_{G,ij}$) corresponding to $M = 3$, where subscript i makes reference to the bit and subscript j to the redundancy number.

3. Results and discussion

We have carried out extensive kinetic Monte Carlo simulations to show that a moderate redundancy leads to enhanced signal processing by reducing the overlapping of the net charge distributions associated with the different bits (see figures 4–6). In every simulation the nanostructure characteristics are changed according to truncated Gaussian distributions with variability width δ. The results are presented in the form of histograms of net charge distributions showing the average values of a large number of simulations. Three cases are considered: no redundancy ($M = 1$), low redundancy ($M = 3$) and moderate redundancy ($M = 6$). The respective numbers of simulations are 400, 500 and 1000 (the number of simulations is increased in this series to obtain meaningful statistics).

Figures 4(a) and (b) show the net charge Q_i delivered by each nanostructure in the case of no redundancy ($M = 1$). Figure 4(b) shows the values of Q_1 (yellow) and Q_2 (red) for $\delta = 0$, obtained with 400 kinetic Monte Carlo simulations, in the form of histograms. The spread around the mean values of Q_1 and Q_2 is due to thermal noise. The tails of the distributions of Q_1 and Q_2 overlap (as shown by the grey vertical strip) and hence the threshold charge is not well defined. This implies that there is a probability that the signal processing gives incorrect results because some Q_1 values are above the threshold charge (shown as a black vertical line). Figure 4(b) shows the values of Q_1 (light blue) and Q_2 (dark blue) for $\delta = 0.2$ in the form of histograms. The distribution widths of Q_1 and Q_2 are now larger due to the combined effects of thermal noise and nanostructure variability. The overlapping of the distribution tails is so large that the signal processing is unreliable under these conditions. Figure 4(a) shows the simulation results in the case of the seven bits for variability widths $\delta = 0$, 0.1, and 0.2. The vertical bars indicate the mean values for the distribution of 400 Q_i values obtained in the simulations. The width of the distributions is shown in the form of segments. The black horizontal line is the threshold charge established to determine the state of bit i: the bit is black if Q_i is above the threshold and white otherwise. It is clear that the mean values of Q_2, Q_3, Q_6, and Q_7 are above the threshold (and hence these are the black bits) but the distribution widths are so large, especially in the case of non-zero variability δ, that a significant fraction of Q_2, Q_3, Q_6, and Q_7 values are below the threshold, which implies unreliable signal processing. Similarly, the distribution widths of Q_1, Q_4, and Q_5 are so large that some values are above the threshold,

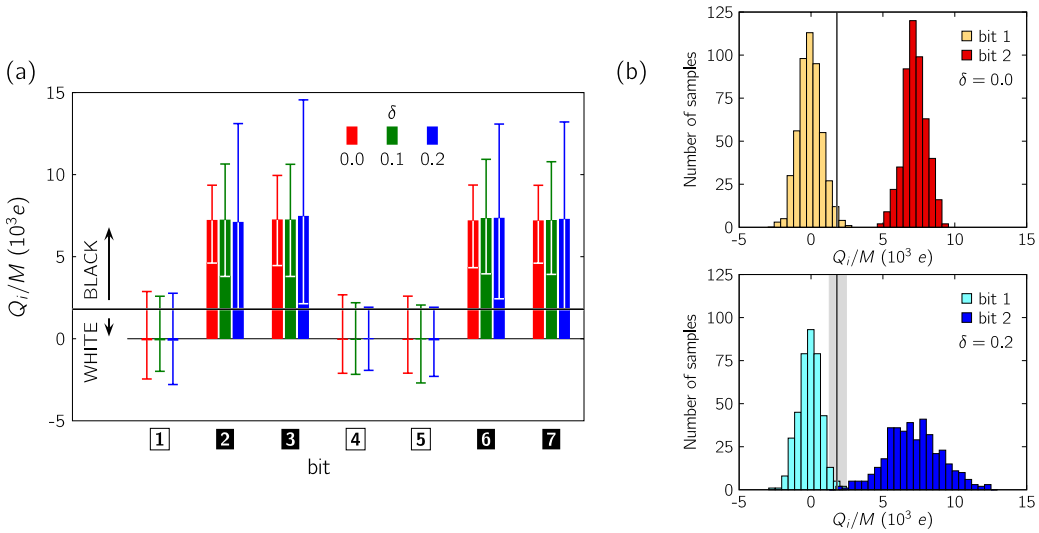

Figure 5. (a) Net charge Q_i/M delivered per nanostructure in the 7 groups of $M = 3$ redundant nanostructures that describe every bit for variability $\delta = 0$, 0.1, and 0.2. (b) Distributions of values of Q_1/M and Q_2/M obtained with 500 simulations for $\delta = 0$ and 0.2. The overlapping region of the distribution tails of Q_1/M and Q_2/M is shown as a grey vertical strip. The black vertical line is the threshold charge.

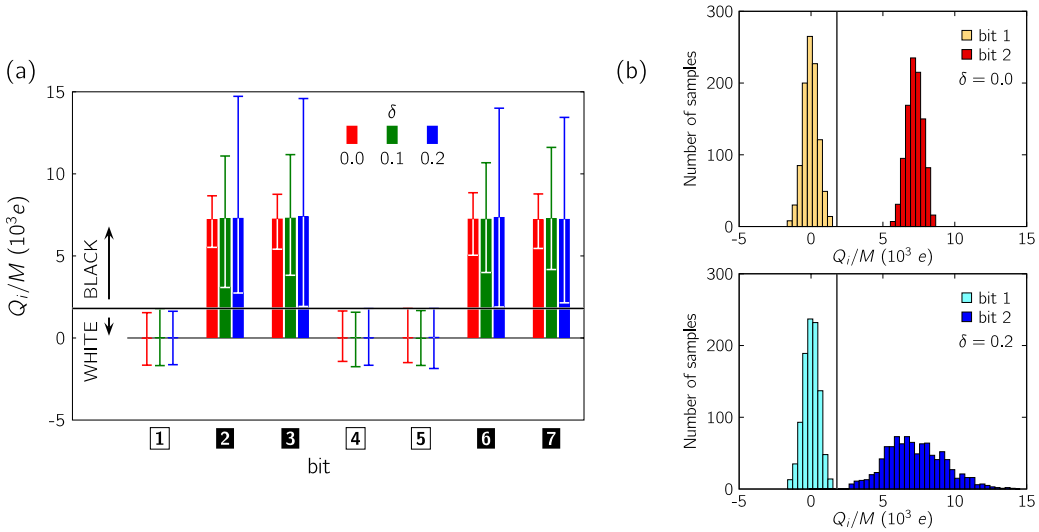

Figure 6. (a) Net charge delivered per nanostructure for a redundancy of $M = 6$ nanostructures per bit and variability $\delta = 0$, 0.1, and 0.2. (b) Distributions of values of Q_1/M and Q_2/M obtained with 1000 simulations for $\delta = 0$ and 0.2. Overlapping is avoided with moderate redundancy, thus achieving efficient signal processing.

leading also to a wrong determination of the bit state. With no redundancy, a good threshold charge cannot be determined because of the significant overlapping of the Q_i distributions.

Figure 5(a) shows the net charge delivered per nanostructure Q_i/M using a low redundancy of $M = 3$ nanostructures per bit. Figure 5(b) shows the Q_i/M distributions of bits 1 and 2 for $\delta = 0$ and 0.2. The signal processing reliability is improved significantly with respect to the case $M = 1$, except for the higher variability $\delta = 0.2$. The width of the Q_i/M distributions increases with δ for black bits and the overlapping region that leads to poor signal processing also widens at high δ.

Figure 6(a) shows the net charge delivered using a moderate redundancy of $M = 6$ nanostructures per bit and figure 6(b) shows the Q_i/M distributions of bits 1 and 2 for $\delta = 0$ and 0.2. It is observed that the reliability of the signal processing scheme is enhanced significantly with a moderate redundancy ($M = 6$).

Figures 4–6 show that circuit redundancy can compensate for a significant variability in the nanostructure characteristics, allowing for efficient signal processing even with non-identical nanostructures. This is emphasized finally in figure 7, corresponding to the difference between the highest value obtained in the simulations for Q_1 ($Q_{1,\max}$) and the minimum value obtained for Q_2 ($Q_{2,\min}$). This difference is scaled to the average value of Q_2 and shown as a function of the redundancy M. There is overlapping between the distributions of Q_1 and Q_2 (and thus unreliable signal processing) when $Q_{1,\max} -$

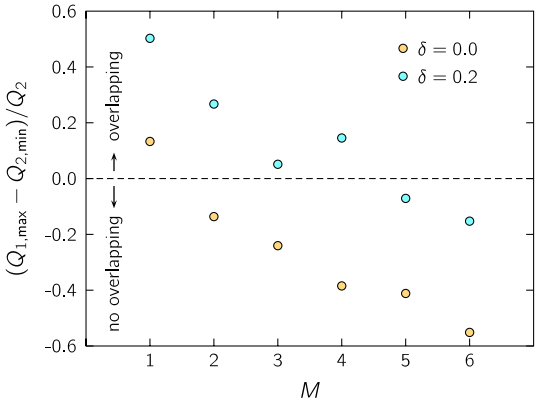

Figure 7. The difference between the highest value obtained for Q_1 ($Q_{1,max}$) and the minimum value obtained for Q_2 ($Q_{2,min}$), scaled to the average value of Q_2, as a function of the redundancy M for two variability values δ. Note that $Q_{1,max} - Q_{2,min}$ indicates the gap between the two distributions: when this difference is negative, a threshold value Q_{th} can be approximately defined to implement reliable signal processing.

$Q_{2,min} > 0$. On the contrary, $Q_{1,max} - Q_{2,min} < 0$ corresponds to a gap between the two distributions (and thus reliable signal processing). Figure 7 clearly shows the significant improvement in the device reliability that is obtained when a moderate redundancy is used in the signal processing system. When the nanostructures are identical ($\delta = 0$), the case $M = 2$ gives a sufficiently high gap between the distributions of Q_1 and Q_2. For systems that suffer from significant variability ($\delta = 0.2$ in figure 7), a higher (but moderate) redundancy is needed. In both cases, $Q_{1,max} - Q_{2,min}$ decreases with M, suggesting that nanostructures with higher variability δ could still be employed by further increasing the values of M.

Note finally that, because of their close proximity, the state of a given nanostructure may be influenced cooperatively by their nearest neighbours in the ensemble of redundant nanostructures that compose every bit. These local interactions could perhaps be exploited to enhance the effect of redundancy [66] and improve further the system reliability.

4. Conclusions

The increasing number of switchable nanostructures that have been demonstrated experimentally is stimulating novel information processing schemes based on these systems. However, because of the fabrication processes at the nanoscale, the building blocks of the new architectures proposed will suffer from a relatively high variability. This variability, together with the thermal noise effect, must be compensated for by using fault-tolerant techniques such as circuit redundancy.

We have recently shown that signal processing can be based on nanoswitches whose conductance is tuned by an external stimulus between two (*on* and *off*) states [30]. This previous work has been extended here to account for the effects of nanostructure variability by using a phenomenological model that includes the stochastic nature of electron transfer and the uncertainties caused by the thermal noise. It is shown that reliable signal processing can still be achieved by adapting the number of building blocks per bit (redundancy) to the nanostructure tolerances (variability). Extensive kinetic Monte Carlo simulations show that a moderate level of redundancy can compensate for significant nanostructure variability in practical operation. This result gives additional support to the concept of *ensembles of redundant nanostructures* for signal processing at the nanoscale.

Acknowledgments

Financial support from the European Commission (project DYNAMO, FP6-028669-2, *New and Emerging Science and Technology* programme) and the Ministry of Science and Innovation of Spain (project MAT2009-07747) and FEDER is acknowledged.

References

[1] Feldheim D 2000 *Nature* **408** 45
[2] Gittins D I, Bethell D, Schiffrin D J and Nichols R J 2000 *Nature* **408** 67
[3] Kornyshev A A, Kuznetsov A M and Ulstrup J 2005 *ChemPhysChem* **6** 583
[4] Terabe K, Hasegawa T, Nakayama T and Aono M 2005 *Nature* **433** 47
[5] Banno N, Sakamoto T, Iguchi N, Sunamura H, Terabe K, Hasegawa T and Aono M 2008 *IEEE Trans. Electron Devices* **55** 3283
[6] Walter D G, Campbell D J and Mirkin C A 1999 *J. Phys. Chem.* B **103** 402
[7] Kudernac T, van der Molen S J, van Wees B J and Jeringa B L 2006 *Chem. Commun.* 3597
[8] Ahonen P, Laaksonen T, Schiffrin D J and Kontturi K 2007 *Phys. Chem. Chem. Phys.* **9** 4898
[9] Tanaka Y, Inagaki A and Akita M 2007 *Chem. Commun.* 1169
[10] Dulic D, van der Molen S J, Kudernac T, Jonkman H T, de Jong J J D, Bowden T N, van Esch J, Feringa B L and van Wees B J 2003 *Phys. Rev. Lett.* **91** 207402
[11] Xu B, Xiao X, Yang X, Zang L and Tao N 2005 *J. Am. Chem. Soc.* **127** 2386
[12] van Dijk E H, Myles D J T, van der Veen M H and Hummelen J C 2006 *Org. Lett.* **8** 2333
[13] Areephong J, Browne W R, Katsonis N and Feringa B L 2006 *Chem. Commun.* 3930
[14] Baron R, Onopriyenko A, Katz E, Lioubashevski O, Willner I, Wang S and Tian H 2006 *Chem. Commun.* 2147
[15] Xie F-Q, Obermair C and Schimmel T 2004 *Solid State Commun.* **132** 437
[16] Jo S H, Kim K-H and Lu W 2009 *Nano Lett.* **9** 496
[17] McCreery R L 2004 *Chem. Mater.* **16** 4477
[18] Chen J, Reed M A, Rawlett A M and Tour J M 1999 *Science* **286** 1550
[19] Chen J, Su J, Wang W and Reed M A 2003 *Physica* E **16** 17
[20] Nishiguchi K and Fujiwara A 2009 *Nanotechnology* **20** 175201
[21] Kim T H, Jang E Y, Lee N J, Choi D J, Lee K-J, Jang J-t, Choi J-s, Moon S H and Cheon J 2009 *Nano Lett.* **9** 2229
[22] Szacilowski K 2008 *Chem. Rev.* **108** 3481
[23] Brust M, Walker M, Bethell D, Schifrin D and Whyman R 1994 *J. Chem. Soc. Chem. Commun.* **7** 801
[24] Chen S, Ingram R S, Hostetler M J, Pietron J J, Murray R W, Schaaff T G, Khoury J T, Alvarez M M and Whetten R L 1998 *Science* **280** 2098
[25] Quinn B M, Liljeroth P, Ruiz V, Laaksonen T and Kontturi K 2003 *J. Am. Chem. Soc.* **125** 6644
[26] Chaki N K, Kakade B, Vijayamohanan K P, Singh P and Dharmadhikari C V 2006 *Phys. Chem. Chem. Phys.* **8** 1837

[27] Garcia-Morales V and Mafé S 2007 *J. Phys. Chem.* C **111** 7242
[28] Schmid G 2001 *Adv. Eng. Mater.* **3** 737
[29] Yamanoi Y and Nishihara H 2007 *Chem. Commun.* 3983
[30] Cervera J, Ramírez P and Mafé S 2008 *J. Appl. Phys.* **104** 084317
[31] Wang W, Lee T and Reed M A 2003 *Phys. Rev.* B **68** 035416
[32] Akkerman H B and de Boer B 2008 *J. Phys.: Condens. Matter* **20** 013001
[33] Blencowe M P 2007 *Contemp. Phys.* **46** 249
[34] Weibel N, Grunder S and Mayor M 2007 *Org. Biomol. Chem.* **5** 2343
[35] Wang Z, Tan B, Hussain I, Schaeffer N, Wyatt M F, Brust M and Cooper A I 2007 *Langmuir* **23** 885
[36] Rose G R, Yao Y, Tour J M, Cabe A C, Gergel-Hackett N, Majumdar N, Bean J C, Harriott L R and Stan M R 2007 *ACM J. Emerg. Technol. Comput. Syst.* **3** 3
[37] Seo K, Konchenko A V, Lee J, Bang G S and Lee H 2008 *J. Am. Chem. Soc.* **130** 2553
[38] Yu Y and Chow W K 2004 *Sensors Actuators* A **116** 79
[39] Nikolic K, Sadek A and Forshaw M 2002 *Nanotechnology* **13** 357
[40] Snider G 2007 *Nanotechnology* **18** 365202
[41] Remacle F, Willner I and Levine R D 2005 *ChemPhysChem* **6** 1239
[42] Kim D-H, Lee H, Song C-K and Lee C 2006 *J. Nanosci. Nanotechnol.* **6** 3470
[43] Rinaldi R and Cingolani R 2004 *Physica* E **21** 45
[44] Nitahara S, Terasaki N, Akiyama T and Yamada S 2006 *Thin Solid Films* **499** 354
[45] Bachtold A, Hadley P, Nakinishi T and Dekker C 2001 *Science* **294** 1317
[46] Javey A, Wang Q, Ural A, Li Y and Dai H 2002 *Nano Lett.* **2** 929
[47] Park W I, Kim J S, Yi G-C and Lee H-J 2005 *Adv. Mater.* **17** 1393
[48] Huang Y, Duan X, Cui Y, Lauhon L J, Kim K-H and Lieber C M 2001 *Science* **294** 1313
[49] Ellenbogen J C and Love J C 2000 *Proc. IEEE* **88** 386
[50] Yamanaka T, Morie T, Nagata M and Iwata A 2000 *Nanotechnology* **11** 154
[51] Berven C A, Wybourne M N, Clarke L, Longstreth L, Hutchinson J E and Mooster J L 2002 *J. Appl. Phys.* **92** 4513
[52] Ami S, Hliwa M and Joachim C 2003 *Chem. Phys. Lett.* **367** 662
[53] Pita M, Krämer M, Zhou J, Poghossian A, Schöning M J, Fernández V M and Katz E 2008 *ACS Nano* **2** 2160
[54] Ferreira R, Remon P and Pischel U 2009 *J. Phys. Chem.* C **113** 5805
[55] Cervera J, Manzanares J A and Mafé S 2009 *J. Appl. Phys.* **105** 074315
[56] Likharev K 1999 *Proc. IEEE* **87** 606
[57] Cervera J and Mafé S 2008 *Chem. Phys. Lett.* **451** 257
[58] Pistolesi F and Fazio R 2005 *Phys. Rev. Lett.* **94** 036806
[59] Mafé S, Manzanares J A and Cervera J 2008 *J. Phys. Chem.* C **112** 1663
[60] Bagrets D A and Nazarov Y V 2003 *Phys. Rev.* B **67** 085316
[61] Pistolesi F 2004 *Phys. Rev.* B **69** 245409
[62] Gorelik L Y, Isacsson A, Voinova M V, Kasemo B, Shekhter R I and Jonson M 1998 *Phys. Rev. Lett.* **80** 4526
[63] Cervera J, Claver J M and Mafé S 2009 *Physica* E **41** 1484
[64] von Neumann J 1956 Probabilistic logics and the synthesis of reliable organisms from unreliable components *Automata Studies* ed C E Shannon and J McCarthy (Princeton: Princeton University Press)
[65] Martorell F, Cotofana S D and Rubio A 2008 *IEEE Trans. Nanotechnol.* **7** 24
[66] Martorell F and Rubio A 2008 *Microelectron. J.* **39** 1041
[67] García-Raya D, Madueño R, Blázquez M and Pineda T 2009 *J. Phys. Chem.* C **113** 8756
[68] Matsuda K, Yamaguchi H, Sakano T, Ikeda M, Tanifuji N and Irie M 2008 *J. Phys. Chem.* C **112** 17005
[69] Mertens S F L, Blech K, Sologubenko A S, Mayer J, Simon U and Wandlowski T 2009 *Electrochim. Acta* **54** 5006
[70] Ganesh K R, Hopson T J, Rawlett A M, Nagahara L A, Primak A and Lindsay S M 2003 *Science* **300** 1413
[71] Haruyama J, Davydov D N, Routkevitch D, Ellis D, Statt B W, Moskovits M and Xu J M 1998 *Solid State Electron.* **42** 1257
[72] Rawlett A M, Hopson T J, Nagahara L A, Tsui R K, Ramachandran G K and Lindsay S M 2002 *Appl. Phys. Lett.* **81** 16
[73] Xu B and Tao N J 2003 *Science* **301** 1221
[74] Loo Y-L, Lang D V, Rogers J A and Hsu J W P 2003 *Nano Lett.* **3** 913